JBC Papers in Press. Published on March 25, 2009 as Manuscript M808116200
The latest version is at http://www.jbc.org/cgi/doi/10.1074/jbc.M808116200

# OXIDATIVE STRESS IS LINKED TO ERK1/2-P16 SIGNALING-MEDIATED GROWTH DEFECT IN ATM-DEFICIENT ASTROCYTES

**Jeesun Kim and Paul KY Wong**

From Department of Carcinogenesis, University of Texas M.D. Anderson Cancer Center, Smithville, Texas, USA

Running head: ROS activates ERK1/2-p16 pathway in *Atm*$^{-/-}$ astrocytes

Address correspondence to: Paul K.Y. Wong, Ph.D. The University of Texas, M.D. Anderson Cancer Center, Science Park - Research Division, 1808 Park Rd., 1C, P.O. Box 389, Smithville, TX 78957 Tel: 512-237-9456; Fax: 512-237-2444; E-mail: pkwong@mdanderson.org

**The gene that encodes the ATM protein kinase is mutated in ataxia-telangiectasia (A-T). One of the prominent features of A-T is progressive neurodegeneration. We have previously reported that primary astrocytes isolated from *Atm*$^{-/-}$ mice grow slowly and die earlier than control cells in culture. However, the mechanisms for this remain unclear. We show here that intrinsic elevated intracellular levels of reactive oxygen species (ROS) are associated with the senescence-like growth defect of *Atm*$^{-/-}$ astrocytes. This condition is accompanied by constitutively higher levels of extracellular signal regulated kinase (ERK) 1/2 phosphorylation and p16$^{Ink4a}$ in *Atm*$^{-/-}$ astrocytes. We also observe that ROS-induced upregulation of p16$^{Ink4a}$ occurs correlatively with ERK1/2-dependent downregulation and subsequent dissociation from chromatin of Bmi-1. Furthermore, both mitogen-activated protein kinase (MEK) inhibitor PD98059 and antioxidant *N*-acetyl-L-cysteine (NAC) restored normal proliferation of *Atm*$^{-/-}$ astrocytes. These results suggest that ATM is required for normal astrocyte growth through its ability to stabilize intracellular redox status, and that inability to control ROS is the molecular basis of limited cell growth of *Atm*$^{-/-}$ astrocytes. This defect may be mediated by a mechanism involving ERK1/2 activation and Bmi-1 de-repression of p16$^{Ink4a}$. These data identify new potential targets for therapeutic intervention in A-T neurodegeneration.**

A prominent feature of ataxia-telangiectasia (A-T) is neurodegeneration that is caused by mutations in the *Atm* (ataxia telangiectasia mutated) gene (1-3). The *Atm* gene product, ATM protein kinase, regulates the cell cycle in response to DNA damage and to oxidative stress (4-5). Within the central nervous system (CNS), proper responses to ROS are required to prevent neurodegeneration (6-9). Others have shown that exogenous antioxidants prevent Purkinje cell death (10) and correct neurobehavioral deficits in *Atm*$^{-/-}$ mice (11-12). These findings suggest that abnormalities in redox status contribute to the A-T phenotype (13-16). Although increased oxidative stress has been shown to characterize ATM deficiency in the CNS, the mechanisms by which oxidative stress promotes neuronal cell loss in A-T remain unclear.

A-T neurodegeneration is primarily due to loss of cerebella Purkinje neurons and to malfunction of other neuronal cells as well (3). Neurons in the CNS depend upon astrocytes for structural, functional and thiol support (17-18). For example, Purkinje neurons in the cerebellum rely heavily on their supporting Bergmann astrocytes (19). We have shown that Bergmann astrocytes of *Atm*$^{-/-}$ mice are under oxidative stress (20), implying that oxidative stress resulting from loss of ATM may promote astrocyte dysfunction. Others have also shown that cultured astrocytes from *Atm*$^{-/-}$ mice have cell cycle and growth defects (21), and that astrocytes isolated from *Atm*$^{-/-}$ mouse embryos grow poorly in culture and readily undergo senescence (15, 20). These observations imply that ATM is essential for normal astrocyte growth and maturation. In light of the importance of astrocytes in supporting neurons against oxidative stress, we hypothesize that aberrant growth and function of *Atm*$^{-/-}$ astrocytes may contribute to neuron loss in A-T.

We show here that *Atm*$^{-/-}$ astrocytes exhibit senescence-like growth arrest, compared with to the growth characteristics of their wild-type (*Atm*$^{+/+}$) counterparts. We also show that elevated ROS levels are one of the causes of proliferation defects in *Atm*$^{-/-}$ astrocytes. This conclusion is based on the observation that defective cell growth of *Atm*$^{-/-}$ astrocytes is restored to normal by the

antioxidant *N*-acetyl-L-cysteine (NAC). This in turn implies that the role of ATM in normal astrocytic proliferation involves stabilization of redox status in the cell. We also observe that growth arrest of $Atm^{-/-}$ astrocytes is associated with chronic maintenance of high levels of the cyclin-dependent kinase inhibitors and phosphorylation of ERK1/2 under conditions in which intracellular ROS levels are elevated. In addition, we identify an intermediate player, Bmi-1, that links ERK1/2 to upregulation of $p16^{Ink4a}$. Bmi-1, a polycomb group RING finger protein 4 has been implicated in proliferation of several cell types, through its transcriptional repression of $p16^{Ink4a}$ (22-23). We observe that ROS-induced Bmi-1 downregulation and dissociation from chromatin are both ERK1/2 dependent. This suggests that the upregulation of $p16^{Ink4a}$ is mediated by a mechanism involving ERK1/2 activation and Bmi-1's loss-of-function as transcription repressor of $p16^{Ink4a}$. Finally, we show that the MEK inhibitor PD98059 reverse $p16^{Ink4a}$ upregulation and chromatin dissociation of Bmi-1. Furthermore, knockdown of $p16^{Ink4a}$ greatly corrected the cell growth defect in $Atm^{-/-}$ astrocytes.These studies identify a role of ATM in controlling normal astrocyte growth and maturation. This is carried out by suppression of oxidative stress-dependent signaling pathways.

## EXPERIMENTAL PROCEDURES

*Mice–*$Atm^{-/-}$ mice were originally generated by C. Barlow (24). For this study, they were purchased from the Jackson Laboratories (Bar Harbor, ME). We genotyped offspring ($Atm^{+/+}$, $Atm^{+/-}$, or $Atm^{-/-}$) by real-time polymerase chain reaction–based assays of mouse tail DNA. Littermates were used as controls in all experiments. Animal care was in accordance with The University of Texas M. D. Anderson Cancer Center guidelines for animal experiments.

*Cells and cell culture*–Immortalized murine C1 astrocytes were maintained in Dulbecco's modified Eagle's medium (DMEM) supplemented with 10% fetal bovine serum (FBS) and antibiotics (100 units/ml penicillin and 100 μg/ml streptomycin) (25). Cells were passaged biweekly and used for experiments while in the exponential growth phase. Primary astrocytes were isolated from 1 to 2-day-old newborn mouse pups by a method described previously (20, 26). Whole brain of each newborn mouse was removed and minced separately in ice-cold DMEM/F12 medium. A single-cell suspension was obtained by passing the minced tissue through a 70-m nylon mesh cell strainer. The cells were plated onto poly-*L*-lysine-coated 10-mm flasks and grown in DMEM/F12 medium, supplemented with 10% FBS, 5 units/ml penicillin, 5 μg/ml streptomycin and 2.5 g/ml Fungizone. The cells were cultured for 4 days in an incubator with 5% $CO_2$ atmosphere at 37°C until reaching confluence. They were passaged by trypsinization. Cells from passages 4 or 5 were used for all experiments. Astrocytes consistently by the fourth or fifth passage were > 99% GFAP positive (27).

*Chemical reagents*–ATM inhibitor KU55933 (10 μM) was purchased from Sigma. MEK inhibitor PD98059 (50 μM) was purchased from BD Biosciences, and antioxidant NAC (4 mM) was kindly provided by M. Yan (M. D. Anderson Cancer Center) (28).

*Analysis of cell senescence*–SA β-*gal assay* kit (Cell Signaling) was used to visualize senescent cells. Astrocytes were cultured in 6-well plates for 2 days, and then fixed after washing twice with PBS. The cells were further incubated for 24 hours in the presence of staining solution-containing X-gal. Senescent cells were distinguished from viable cells using β-*galactosidase, which* is blue under the microscope.

*Analysis of intracellular ROS*–Intracellular ROS accumulation was monitored by using 2'-7'-dichlorofluorescene diacetate ($H_2$DCFDA), which forms a fluorescent compound, dichlorofluorescein, upon oxidation with ROS. After 30 minutes of incubation in 10 μM $H_2$DCFDA, cells were rinsed twice with phosphate-buffered saline solution (PBS). Fluorescence was monitored by scanning the whole well using a NucleoCounter (New Brunswick Scientific Co., Ltd.) set at excitation and emission wavelengths of 485 and 535 nm.

*Protein analysis*–Cells (1-5 x $10^6$) were seeded into 10-cm dishes, grown to 70%

confluence, and treated with $H_2O_2$ at different concentrations. At 1, 4 or 16 hours after $H_2O_2$ treatment, the cells were washed twice with ice-cold PBS and then scraped directly into lysis buffer containing 150 mM NaCl, 0.5% w/v sodium dodecyl sulfate (SDS), 0.5% v/v NP40, 0.5% w/v sodium deoxycholate, 1 mM EGTA, and a mixture of protease inhibitors (Complete Mini tablets; Boehringer Mannheim). Protein concentrations were determined using a Bradford reagent (BioRad). Protein lysates (30 μg) were separated by SDS polyacrylamide gel electrophoresis on a 12% gel, and transferred to polyvinylidene difluoride membrane. Antibodies used for western-blotting analysis were anti-ERK1/2, anti-phospho-ERK1/2 (Thr202/Tyr204), anti-phospho-Rb (Ser807/811), anti-PCNA, and anti-$p27^{kip1}$ (Cell Signaling Technology); anti-Bmi-1 (Upstate Biotechnology); anti-$p21^{cip1}$, anti-$p16^{Ink4a}$ and anti-actin (Santa Cruz Biotechnology).

*SiRNA-mediated knockdown*–For siRNA knockdown of *Atm*, cells were transfected for 48 hours with 20 nM siRNA (mouse-specific *Atm*) in medium containing 10% (v/v) FBS using Lipofectamine reagent (Invitrogen) according to the manufacturer's protocol for cells. Validated siRNA (SMARTpool) was obtained from Dharmacon. The negative control siRNA used was siCONTROL, which contains at least 4 mismatches to all known human, mouse, and rat genes. For mock transfection, we used siRNA suspension buffer and Lipofectamine containing no siRNA. For siRNA knockdown of $p16^{Ink4a}$, mouse-specific $p16^{Ink4a}$ siRNA was purchased from Santa Cruz Biotechnology.

*Immunofluorescence*–The cells were fixed with 4% paraformaldehyde in PBS for 30 minutes at room temperature, and then permeabilized with 0.1% Triton X-100 in PBS for 15 minutes. For staining with antibodies, cells were incubated for 2 hours at 37°C with 10% FBS in PBS. Primary antibodies were added, and the cells were incubated at 4°C overnight. The cells were then washed three times in PBS/0.1% Triton X-100 for 5 minutes each, and fluorescent secondary antibodies were added for 1 hour at 37°C. The nuclei were stained with 4′, 6-diamidino-2-phenylindole, and slides were mounted in Slowfade (Molecular Probes). Cells were imaged under an Olympus IX2-SL microscope equipped with a ×400 objective and an Olympus DP 70 digital camera connected to a PC computer.

*Statistics*–For each experiment, data are presented as the mean ± S.D. of values. Each experiment was repeated at least three times. Statistical comparisons of values for $Atm^{+/+}$ *vs*. $Atm^{-/-}$ mice, and for untreated control *vs*. treated samples were made using the Mann-Whitney *U* test. Differences were considered significant when $p < 0.05$.

## RESULTS

*Loss of ATM impairs proliferation in astrocytes*–We have reported previously that ATM-deficient primary astrocytes grow slowly, become senescent, and die in culture (20). These results are consistent with those reported by Gosink et al (21). To compare the rate of proliferation of $Atm^{+/+}$ and $Atm^{-/-}$ astrocytes, we analyzed their cell growth curves. As shown in Fig. 1A, $Atm^{-/-}$ astrocytes proliferated much more slowly than $Atm^{+/+}$ astrocytes. In particular, $Atm^{+/+}$ astrocytes show 2.5-3 times higher rates of proliferation than $Atm^{-/-}$ astrocytes at 4 and 5 days after subculturing. When monolayer of $Atm^{+/+}$ and $Atm^{-/-}$ astrocytes were observed under the microscope following further incubation for 4 days, $Atm^{-/-}$ astrocytes showed lower densities than wild type control cells with a decrease of ~50% in cell number (Fig. 1B, left panel). This is consistent with our findings for C1 astrocytes, a murine immortalized astrocyte cell line (25). While the ATM inhibitor, KU55933 slightly decreases astrocytes proliferation, loss of ATM by ATM–small interfering RNA (ATM–siRNA) reduced cell proliferation by ~40% (Fig. 1B, right panel). To obtain direct evidence that ATM deficiency causes cell senescence, a specific senescence–associated *β–galactosidase* (SA *β–gal*) assay was performed after 2-days of culture. Fig. 1C shows that senescent cells are present 2 times more in $Atm^{-/-}$ astrocyte cultures than $Atm^{+/+}$ cultures. These data indicate that ATM deficiency causes the senescent-like cell growth defect in $Atm^{-/-}$ astrocytes.

*Decreased proliferation in $Atm^{-/-}$ astrocytes is caused by elevated ROS levels*–ATM monitors cellular redox status in addition to its monitoring of DNA damage and genomic instability (26), and cells lacking ATM show ROS accumulation (29). Although we have previously shown that loss of *Atm* results in oxidative damage in the brain (20), the involvement of oxidative stress in defective astrocyte growth in the ATM-deficient mouse has not been tested. To address this issue, we compared intracellular ROS levels in $Atm^{+/+}$ and $Atm^{-/-}$ astrocytes by 2'-7'-dichlorofluorescene diacetate ($H_2$DCFDA) staining of intracellular $H_2O_2$. The data show that the intracellular levels of ROS are significantly higher in $Atm^{-/-}$ astrocytes than in $Atm^{+/+}$ astrocytes, and that antioxidant NAC reduces the elevated ROS levels of $Atm^{-/-}$ astrocytes to normal levels (Fig. 2A). This result suggests that elevated ROS levels are intrinsic characteristics of cells lacking ATM. This is consistent with our results from C1 astrocytes treated with ATM specific inhibitor, KU55933, which show higher levels of intracellular ROS compared to untreated control cells (data not shown). For direct evidence that defective proliferation of $Atm^{-/-}$ astrocytes is due to elevated ROS levels, we treated $Atm^{-/-}$ astrocytes with NAC and compared their proliferation rates to those of untreated cells. Figure 2B shows that proliferation rates for $Atm^{-/-}$ astrocytes were increased by treatment with NAC, showing nearly 2-2.5 times higher rates than untreated $Atm^{-/-}$ counterpart at 3 and 4 days after subculturing. This effect of NAC was confirmed by photomicrograph, which disclosed increased cell density by NAC (Fig. 2C). This is consistent with our findings that NAC decreases the proportion of senescent cells in $Atm^{-/-}$ astrocyte cultures (Fig. 2D). These results provide strong evidence linking defective growth of $Atm^{-/-}$ astrocytes to elevated intracellular ROS.

*$H_2O_2$-treated $Atm^{+/+}$ astrocytes show reduced proliferation and upregulated levels of CDK inhibitors*–To determine whether $H_2O_2$ decreases $Atm^{+/+}$ astrocyte proliferation and whether antioxidant inhibits ROS-mediated defective proliferation in normal $Atm^{+/+}$ astrocytes subjected to exogenous oxidative stress, we exposed $Atm^{+/+}$ astrocytes to $H_2O_2$ and treated the same $H_2O_2$-exposed cells with NAC. Figure 3A shows that $H_2O_2$ elevated intracellular ROS levels in $Atm^{+/+}$ astrocytes, and that treatment of $Atm^{+/+}$ astrocytes with NAC reduced their intracellular ROS to normal levels. $Atm^{+/+}$ astrocytes also showed significantly decreased proliferation 2 days after $H_2O_2$ treatment, but $H_2O_2$-induced defective proliferation was partially restored by NAC (Fig. 3B). Treatment with $H_2O_2$ for 2 days followed by 1 day of incubation in $H_2O_2$-free medium induced SA *β-galactosidase* expression in ~40% of $Atm^{+/+}$ astrocytes, but NAC significantly prevented $H_2O_2$-induced senescence (Fig. 3C). These results indicate that $H_2O_2$ inhibits astrocytes proliferation through elevating intracellular ROS, regardless of their ATM status.

We then investigated the effects of ROS on several known key intermediates associated with cell proliferation. The inhibitors of cyclin-dependent kinases (CDK) are considered to play an important role in cell cycle arrest and premature senescence (30). Others have shown that the CDK inhibitor $p21^{cip1}$ is upregulated in $Atm^{-/-}$ astrocytes (26). Therefore, we investigated the effects of ROS on levels of CDK inhibitors, including $p16^{Ink4a}$, $p19^{Arf}$, $p21^{cip1}$, and $p27^{Kip1}$ in $Atm^{+/+}$ astrocytes. $H_2O_2$ treatment of $Atm^{+/+}$ astrocytes stimulated expression of $p21^{cip1}$ and $p16^{Ink4a}$, but not $p27^{kip1}$ in $Atm^{+/+}$ astrocytes (Fig. 3D, upper & lower panel). However, no $p19^{Arf}$ band was present in the lysates from those cells. These alterations indicate that activation of the $p16^{Ink4a}$ and/or $p19^{Arf}$-$p21^{cip1}$ senescence pathway(s) may be involved in ROS-mediated senescence in astrocytes. Furthermore, activation of $p16^{Ink4a}$ was attenuated by NAC (Fig. 3E). These findings suggest that intracellular ROS-mediated oxidative stress induces senescence in astrocytes via activation of the $p16^{Ink4a}$ pathway.

*In $Atm^{-/-}$ astrocytes, ERK1/2 is constitutively activated and CDK inhibitors are upregulated*–We have previously reported that ERK1/2 is activated in both $Atm^{-/-}$ astrocytes in culture and in Bergmann glia in the cerebella of $Atm^{-/-}$ mice (20). We consistently observed higher level of phospho-ERK1/2 in $Atm^{-/-}$ astrocytes than in $Atm^{+/+}$ astrocytes. In addition, Bmi-1, a polycomb ring finger oncogene product is downregulated in $Atm^{-/-}$ cells (Fig. 4A), which is consistent with the fact that Bmi-1 promotes cell proliferation via repression of CDK inhibitors. In figure 3D, we have shown that intracellular ROS

levels increased in *Atm*$^{-/-}$ astrocytes and $H_2O_2$ upregulated CDK inhibitors. We therefore reasoned that CDK inhibitors might be upregulated to decrease proliferation in *Atm*$^{-/-}$ astrocytes. We thus compared the basal levels of CDK inhibitors in *Atm*$^{-/-}$ astrocytes to those in wild-type control cells. Figure 4B shows that the basal expression levels of p53, p21$^{cip1}$, and p16$^{Inka}$ were higher in *Atm*$^{-/-}$ cells than in the wild-type cells. p16$^{Ink4a}$ was upregulated *Atm*$^{-/-}$ cerebella tissues. Not surprisingly, *Atm*$^{-/-}$ astrocytes show lower levels of *Retinoblastoma* (Rb) phosphorylation than do wild type control cells. Moreover, Bmi-1 levels were significantly downregulated in the *Atm*$^{-/-}$ tissues (Fig. 4C, left & right panel).

We next compared p16$^{Ink4a}$ levels in *Atm*$^{-/-}$ astrocytes and *Atm*$^{+/+}$ astrocytes, to which exogenous $H_2O_2$ had been added to the cultures. Interestingly, addition of $H_2O_2$ caused a brief upregulation of p16$^{Inka}$ at 4 hours in wild-type control cells, but then reversed itself down to the untreated basal level at 16 hours post treatment. However, when *Atm*$^{-/-}$ astrocytes were exposed to $H_2O_2$, the level of p16$^{Ink4a}$ expression was further elevated, and this upregulation persisted from 4 to 16 hours post $H_2O_2$ treatment. This means that oxidative stress due to elevated ROS is reversible to normal levels when ATM kinase is present. in both *Atm*$^{+/+}$ and *Atm*$^{-/-}$ astrocytes, Bmi-1 was downregulated in response to $H_2O_2$, but its level was lower in *Atm*$^{-/-}$ astrocytes than in *Atm*$^{+/+}$ astrocytes (Fig. 4D). In *Atm*$^{+/+}$ astrocytes, the brief expression of p16$^{Ink4a}$ may shut down cell cycling, allowing time for the cells to repair any damage. Once the job is done, their levels return to normal, as a result of ATM's redox balancing action.

Figure 4E shows that in both *Atm*$^{+/+}$ and *Atm*$^{-/-}$ astrocytes, $H_2O_2$ treatment also causes phosphorylation of ERK1/2 and upregulation of p16$^{Ink4a}$. Phospho-ERK1/2 and p16$^{Ink4a}$ changes occurred in $H_2O_2$-treated *Atm*$^{+/+}$ astrocytes were less pronounced than in $H_2O_2$-treated *Atm*$^{-/-}$ astrocytes. *Atm*$^{-/-}$ astrocytes also show lower levels of Rb phosphorylation than do wild type control cells. Moreover, Rb phosphorylation was further reduced after $H_2O_2$ exposure. These results indicate that *Atm*$^{-/-}$ astrocytes are differentially hypersensitive to oxidative stress, and maintain high expression levels of phospho-ERK1/2 and p16$^{Ink4a}$. If oxidative stress is prolonged, as it is in cells lacking ATM, upregulation of phospho-ERK1/2 persistently may increase p16$^{Ink4a}$ expression, resulting in prolonged cell cycle arrest and retardation of cell proliferation. These data strongly implicate the involvement of ERK1/2-p16$^{Ink4a}$ signaling pathway in ROS-induced cell growth arrest of *Atm*$^{-/-}$ astrocytes.

*ERK1/2 signaling mediates Bmi-1 downregulation and chromatin dissociation in Atm*$^{-/-}$ *astrocytes*–We next set out to identify the molecular mechanisms underlying the effects of ROS on the cell growth defects of *Atm*$^{-/-}$ astrocytes, focusing on the mechanisms for phospho-ERK1/2 and p16$^{Ink4a}$ upregulation. p16$^{Ink4a}$ expression is known to be regulated by the mitogen-activated protein kinase (MAPK) pathways, including activation of ERK1/2 (31). Furthermore, exposure to $H_2O_2$ activates MAPKs in many cell types (32, 33). Therefore, we tested the effect of ROS on ERK1/2 downstream mediators. Upon phosphorylation at two amino acids (Thr202/Tyr204), ERK1/2 translocates into the nucleus, where it phosphorylates its substrates. Since p16$^{Ink4a}$ expression level does not depend on phosphorylation by ERK1/2, it is not a direct substrate of activated ERK1/2. Instead, p16$^{Ink4a}$ expression is negatively regulated by Bmi-1 (34). Amino acid sequence analysis indicates that Bmi-1 has two predicted consensus motifs for ERK1 phosphorylation (http://www.scansite. mit.edu). We thus asked whether ROS-induced ERK1/2 signaling has effects on Bmi-1 function as a transcription repressor for p16$^{Ink4a}$.

The polycomb group (PcG) proteins including Bmi-1 function as transcription repressors. Chromatin association of these proteins can be demonstrated by puncta in the nucleus in previous study (35). Immunofluorescence imaging of endogenous Bmi-1 in *Atm*$^{+/+}$ astrocytes indicates that Bmi-1 localizes mainly in chromatin, and that it dissociates from chromatin after cells are exposed to $H_2O_2$ with a concomitant upregulation of p16$^{Ink4a}$ (Fig 5A). Bmi-1/chromatin association correlates with trimethylation at the lysine 27 residue of histone H3 (H3K27me3, data not shown), since H3K27me3 is required for polycomb/histone H3 interaction (36). However, it was also noted that Bmi-1/chromatin association does not correlate

with sites of DNA double strand breaks, since fluorescence images of 53BP1 did not colocalize with Bmi-1 in astrocytes treated with $H_2O_2$ (Fig. 5B).

We next asked whether $H_2O_2$-induced Bmi-1/chromatin dissociation is dependent on ERK1/2 signaling. We thus pretreated $Atm^{+/+}$ astrocytes with MEK inhibitor PD98059 before $H_2O_2$ treatment, since MEK is known as the upstream of ERK1/2 (32). Figure 5C shows that $H_2O_2$-induced Bmi-1/chromatin dissociation is significantly inhibited by PD98059. This suggests that Bmi-1 dissociation from chromatin occurs via ERK1/2 signaling. In addition, $H_2O_2$ inhibits astrocyte proliferation, but PD98059 partially rescues it (Fig. 5D). Taken together with increased proliferation by PD98059, reversion of chromatin dissociation and restoration of Bmi-1 by PD98059 indicate that $H_2O_2$-induced proliferation decrease is associated to Bmi-1 dysfunction by ERK1/2 signaling.

Next, we assessed the effect of ATM deficiency on endogenous Bmi-1 localization using $Atm^{-/-}$ astrocytes. Figure 5F shows that Bmi-1 is downregulated, and less Bmi-1 associate with chromatin in $Atm^{-/-}$ astrocytes than does in $Atm^{+/+}$ astrocytes. These results are consistent with previous findings of Bmi-1 downregulation and $p16^{Ink4a}$ upregulation that occur in $Atm^{-/-}$ astrocytes (Fig. 4A). The data link $p16^{Ink4a}$ upregulation to Bmi-1 downregulation in $Atm^{-/-}$ astrocytes, in turn also link these two events to elevated intracellular ROS levels. Since PD98059 also restored normal Bmi-1 and $p16^{Ink4a}$ levels in $Atm^{-/-}$ astrocytes, we conclude that ERK1/2 mediates Bmi-1 downregulation and chromatin dissociation, as well as $p16^{Ink4a}$ upregulation.

*Restoration of normal proliferation of $Atm^{-/-}$ astrocytes by inactivation of ERK1/2 signaling or knockdown of $p16^{Ink4a}$*–We next asked whether activation of ERK1/2 impaires survival and proliferation of $Atm^{-/-}$ astrocytes, and whether inhibiting ERK1/2 signaling restores defective cell growth. We established cultures of $Atm^{-/-}$ astrocytes in the presence of PD98059. Growth curve analysis for 5 days showed that PD98059 partially rescued $Atm^{-/-}$ astrocytes from defective proliferation (Fig. 6A). The restorative actions of PD98059 were also evident in culture, as shown by increase in cell density (Fig. 6B). However, the positive effect of PD98059 on proliferation of $Atm^{-/-}$ astrocytes was not comparable to that of the antioxidant NAC. In addition, PD98059 appeared to inhibit mitogenic pathways in $Atm^{+/+}$ astrocytes, since it reduced growth rate and proliferation in these cells. In normal $Atm^{+/+}$ mice, most astrocytes are quiescent, and thus ERK1/2 signaling is suspended in an inactive state. However, $Atm^{-/-}$ astrocytes maintain constitutive ERK1/2 signaling, associated with oxidative stress-condition.

In spite of its inhibitory effect on $Atm^{+/+}$ astrocytes proliferation, PD98059 partially restored Bmi-1 levels in $Atm^{-/-}$ astrocytes. In addition, both NAC and PD98059 reduced levels of $p21^{cip1}$ and $p16^{Ink4a}$ in $Atm^{-/-}$ astrocytes to levels similar to those in $Atm^{+/+}$ astrocytes. In accordance of these results, level of phospho-Rb was also increased by NAC and PD98059 (Fig. 6C). These results provide direct evidence linking defective growth of $Atm^{-/-}$ astrocytes to activation of ERK1/2 signaling as a result of oxidative stress. However, PD98059 has modest and partial rescuing effect on $Atm^{-/-}$ astrocytes proliferation, indicating that there may be additional pathways associated with defective proliferation in $Atm^{-/-}$ astrocytes.

Since increases in cell senescence and $p16^{Ink4a}$ level were observed in $Atm^{-/-}$ astrocytes, we next decided to access whether $p16^{Ink4a}$ upregulation is responsible for inducing cell senescence, and whether inhibition of $p16^{Ink4a}$ expression would reverse the defective growth phenotype of $Atm^{-/-}$ astrocytes. Ink4a was knockdowned in both $Atm^{+/+}$ and $Atm^{-/-}$ astrocytes using siRNA against mouse $p16^{Ink4a}$. Figure 6D shows that more senescent cells were observed in $Atm^{-/-}$ astrocytes than in $Atm^{+/+}$ astrocytes. However, $Atm^{-/-}$ astrocytes when $p16^{Ink4a}$ was knockdowned had fewer senescent cells than did these cells whose $p16^{Ink4a}$ was intact.

## DISCUSSION

In A-T patients, Purkinje neuron loss in the cerebellum is the most critical feature of the neuropathological phenotype (37). Up to now, therefore, most studies have focused on the effects of ATM deficiency in neurons, with the role(s) of astrocytes going unexplored. However, accumulating evidence now suggests that astrocytes are key elements serving pivotal functions in the central nervous system, including

structural and redox support for neuron, neurotransmitter synthesis, and transport of nutrients and metabolic precursors to neurons (17, 19, 38-40). Previous studies have reported that transgenic and knockout mouse models for certain astrocyte-specific proteins result in neurodegenerative disorders (41-42). This implies that abnormalities in astrocytes might also cause neuropathophysiology of A-T. This is consistent with earlier observations by others that Purkinje cell survival in *Atm*-deficient mice is partially reversed when these cells are cultured in the presence of $Atm^{+/+}$ astrocyte-conditioned medium (18). It will be important now to determine whether $Atm^{-/-}$ astrocytes have cytotoxic effects for neurons in co-culture. Studies now in progress in our lab will address effects of $Atm^{-/-}$ astrocytes on neurons in this context.

At normal concentrations, ROS play a role in cellular functions involving signal transduction (43-44). However, an imbalance between generation of ROS and capacity of antioxidants to neutralize ROS can result in disruption of cellular redox status, leading to oxidative stress (45-47). Mammalian cells have therefore evolved a wide range of mechanisms, including ATM, for maintaining normal levels of intracellular ROS. Neuronal cells require large quantities of oxygen to function because of their high metabolic rate. As a result, neurons generate high levels of ROS. For this reason, the CNS is very vulnerable to ROS imbalance and accumulation. In general, low doses of $H_2O_2$ promote cell proliferation, whereas high levels of ROS elicit cell cycle arrest, senescence, and apoptosis (48). Our data show that $Atm^{-/-}$ astrocytes have a lower proliferation rate than that of normal cells. We previously observed increased spontaneous DNA synthesis in cultured $Atm^{-/-}$ astrocytes relative to $Atm^{+/+}$ astrocyte in spite of their decreased proliferation (20). The reason for this discrepancy is unknown. However, it is possible that abnormally elevated DNA synthesis in $Atm^{-/-}$ astrocytes may occur without cell division. This is in turn could elevate ROS production in the cells (15).

Our observation that $p21^{Cip1}$ is upregulated in $Atm^{-/-}$ astrocytes (Fig. 4B) and that PD98059 inhibits $p21^{Cip1}$ upregulation (data not shown) are consistent with those from a previous study (26). The *Ink4a/Arf* locus encodes two proteins, $p16^{ink4a}$ and $p19^{arf}$, by alternative splicing (49-51). *Ink4a* and *Arf* are important components in Rb and p53 pathways, respectively, and both proteins function in cell cycle regulation (52-53). Bmi-1 is a potent repressor of both *Ink4a* and *Arf*. Our data suggest that Bmi-1 downregulation and dissociation from chromatin with resultant $p16^{Ink4a}$ upregulation may contribute to the defective proliferation and premature senescence of $Atm^{-/-}$ astrocytes. A very interesting observation made by other researchers is that *Bmi-1* knockout mice progressively develop A-T-like motor abnormalities, such as ataxia (22). This information substantiates the observations reported above, and supports the idea that CNS pathology is similar if either ATM or Bmi-1 is absent. Since derepression of the Ink4a/Arf gene locus has been correlated with *Bmi-1*-deficient phenotypes in the nervous system, it is important to determine whether the deletion of both *Ink4a* and *Arf* genes restores functions of $Atm^{-/-}$ astrocytes. Notably, we observed that knockdown of Ink4a restores proliferation of $Atm^{-/-}$ astrocytes (Fig. 6D). Furthermore, work by others has also shown that the A-T like motor abnormalities observed in *Bmi-1* knockout mice restored in $Bmi\text{-}1^{-/-}/p16^{Ink4a\text{-}/\text{-}}$ double knockout mice (54). This result further substantiates that $p16^{Ink4a}$ plays a role in *Bmi-1* deficient condition.

We have shown that Bmi-1/chromatin association is disrupted by $H_2O_2$ (Fig. 5A, B, &C). Previous studies on Bmi-1 have reported that its function as transcription repressor is regulated by its phosphorylation status (35). Since Bmi-1 contains two predicted ERK1 phosphorylation sites, we asked whether Bmi-1 phosphorylation is induced by oxidative stress, and whether it is ERK1/2 dependent. We reasoned that ROS-induced phosphorylation of Bmi-1 may directly or indirectly contribute to its chromatin dissociation, which in turn would result in de-repression of $p16^{Ink4a}$. Since no specific antibody is available to detect phosphorylated form of Bmi-1, its phosphorylation was determined by mobility shift on gels in the presence of phosphatase inhibitors. These experiments demonstrated that $H_2O_2$ treatment causes the mobility shift of Bmi-1 (data not shown). However, even though downregulation and chromatin dissociation of Bmi-1 occur in $Atm^{-/-}$ astrocytes, no intrinsic difference in Bmi-1 phosphorylation is observed between $Atm^{+/+}$ and $Atm^{-/-}$ astrocytes in western-blotting analysis (Fig. 4A). This might be

explained by the fact that the mobility shift of Bmi-1 is able to be detected for only short time after $H_2O_2$ treatment, after which time Bmi-1 levels decreased (Fig. 4D). Therefore, it is possible that phosphorylation of Bmi-1 may lead to its degradation. It will be interesting to determine whether inhibition of proteasomal degradation restores functions of *Atm*$^{-/-}$ astrocytes by preventing Bmi-1 degradation.

In recent years, accumulating evidence has indicated that protein kinase activities are redox-sensitive because key cysteine residues in these proteins can undergo posttranslational modifications by oxidants. $H_2O_2$-induced formation of disulfide bonds in protein kinases has been documented, suggesting that kinases function as redox sensors and that $H_2O_2$-induced conformational changes or formation of dimers from disulfide bonds triggers kinase activation (45, 55). This is consistent with our observation that ATM is activated in response to $H_2O_2$ (data not shown). Although at present the mechanism of how $H_2O_2$-induced ERK1/2 activation is unclear, we speculate that a candidate upstream mediator, such as receptor tyrosine kinase (RTK) may be responsible for $H_2O_2$-induced ERK1/2 activation, since others have shown that upstream RTK may act as a trigger for such events (56). Our further studies will address the role of RTK in modulating $H_2O_2$-induced ERK1/2 signaling.

In conclusion, our data demonstrate that ATM is required to maintain normal growth of astrocytes by controlling intracellular levels of ROS. The absence of ATM limits the growth of astrocytes through ERK1/2-dependent mechanisms, including downregulation and chromatin dissociation of Bmi-1, and subsequent upregulation of p16$^{Ink4a}$. The events are prevented by antioxidants and inhibited by inactivation of MEK, which is upstream of ERK1/2 (Fig.7). These data therefore identify a novel mechanism by which ATM deficiency leads to the astrocytes growth arrest, and they identify new targets for effective pharmacological intervention in A-T patients.

## REFERENCES


1. Savitsky, K., Bar-Shira, A., Gilad, S., Rotman, G., Ziv, Y., Vanagaite, L., Tagle, D.A., Smith, S., Uziel, T., Sfez, S., Ashkenazi, M., Pecker, I., Frydman, M., Harnik, R., Patanjali, S.R., Simmons, A., Clines, G.A., Sartiel, A., Gatti, R.A., Chessa, L., Sanal, O., Lavin, M.F., Jaspers, N.G., Taylor, A.M., Arlett, C.F., Miki, T., Weissman, S.M., Lovett, M., Collins, F.S., and Shiloh, Y. (1995) *Science* **268**, 1749-1953
2. Jorgensen, T.J., and Shiloh, Y. (1996) *Int. J. Radiat. Biol.* **69**, 527-537
3. Crawford, T.O. (1998) *Semin. Pediatr. Neurol.* **5**, 287-294
4. Shiloh, Y., and Rotman, G. (1996) *J. Clin. Immunol.* **16**, 254-260
5. Shiloh, Y. (2003) *Nat. Rev. Cancer* **3**, 155-168
6. Lucius, R., and Sievers, J. (1996) *Brain Res*. **743**, 56-62
7. Campese, V.M., Ye, S., Zhong, H., Yanamadala, V., Ye, Z., and Chiu, J. (2004) *Am. J. Physiol. Heart. Circ. Physiol.* **287**, 695-703
8. Leutner, S., Schindowski, K., Frölich, L., Maurer, K., Kratzsch, T., Eckert, A., and Müller W.E. (2005) *Parmacopsychiatry* **38**, 312-315
9. Jiang, Y., Scofield, V. L., Yan, M., Qiang, W., Liu, N., Reid, A. J., Lynn, W. S., and Wong, P. K. Retrovirus-induced oxidative stress with neuroimmunodegeneration is suppressed by antioxidant treatment with a refined monosodium alpha-luminol (Galavit). *J. Virol.*, **80**, 4557-4569
10. Chen, P., Peng, C., Luff, J., Spring, K., Watters, D., Bottle, S., Furuya, S., and Lavin, M.F. (2003) *J. Neurosci.* **23**, 11453-11460
11. Browne, S.E., Roberts, L.J.II, Dennery, P.A., Doctrow, S.R., Beal, M.F., Barlow, C., and Levine, R.L. (2004) *Free. Radic. Biol. Med.* **36**, 938-942
12. Gueven, N., Luff, J., Peng, C., Hosokawa, K., Bottle, S.E., and Lavin, M.F. (2006) *Free Radic. Biol. Med.* **41**, 992-1000
13. Rotman, G., and Shiloh, Y. (1997) *Cancer Surv.* **29**, 285-304
14. Reichenbach, J., Schubert, R., Schindler, D., Muller, K., Bohles, H., and Zielen, S. (2002) *Antioxid.*

*Redox Signal*. **4**, 465-469
15. Watters, D.J. (2003) *Redox Rep*. **8**, 23-29
16. Barzilai, A., and Yamamoto, K. (2004) *DNA Repair* **3**, 1109-1115
17. Wong, P.K.Y., and Lynn, W.S. (1997) *J. Immunol. Immunophamacol.* **17**, 30-35
18. Wang, X.F., and Cynader, M.S. (2000) *J. Neurochem.* **74**, 1434-1442
19. Takuma, K., Baba, A., and Matsuda, T. (2004) *Prog. Neurobiol.* **72**, 111-127
20. Liu, N., Stoica, G., Yan, M., Scofield, V.L., Qiang, W., Lynn, W.S., and Wong, P.K.Y. (2005) *Lab. Invest.* **85**, 1471-1480
21. Gosink, E.C., Chong, M.J., and McKinnon, P.J. (1999) *Cancer Res*. **59**, 5294-5298
22. Molofsky, A.V., He, S., Bydon, M., Morrison, S.J., and Pardal, R. (2005) *Genes Dev*. **19**, 1432-1437
23. Pardal, R., Molofsky, A.V., He, S., and Morrison, S.J. (2005) *Cold Spring Harb. Symp. Quant. Biol.* **70**, 177-185
24. Barlow, C., Hirotsune, S., Paylor, R., Liyanage, M., Eckhaus, M., Collins, F., Shiloh, Y., Crawley, J.N., Ried, T., Tagle, D., and Wynshaw-Boris, A. (1996) *Cell* **86**, 159-171
25. Lin, Y.C., Chow, C.W., Yuen, P.H., and Wong, P.K.Y. (1997) *J. Neurovirol.* **3**, 28-37
26. Lee, Y., Chong, M.J., and McKinnon, P.J. (2001) *J. Neurosci*. **21**, 6687-6693
27. Shikova, E., Lin, Y.C., Saha, K., Brooks, B.R., and Wong, P.K.Y. (1993) *J. Virol.* **67**, 1137-1147
28. Yan, M., Zhu, C., Liu, N., Jiang, Y., Scofield, V.L., Riggs, P.K.Y., Qiang, W., Lynn, W.S., and Wong, P.K.Y. (2006) *Free. Radic. Biol. Med*. **41**, 640-648
29. Barzilai, A., and Yamamoto, K. (2004) *DNA Repair* **3**, 1109-1115
30. Collado, M., Blasco, M.A., and Serrano, M. (2007) *Cell* **130**, 223-233
31. Wen-Sheng, W. (2003) *Oncogene* **22**, 955-963
32. Bartov, O., Sultana, R., Butterfield, D.A., and Atlas, D. (2006) *Brain Res.* **1069**, 198-206
33. Moors, M., Cline, J.E., Abel, J., and Fritsche, E. (2007) *Toxicol. Appl. Pharmacol.* **221**, 57-67
34. Vonlanthen, S., Heighway, J., Altermatt, H.J., Gugger, M., Kappeler, A., Borner, M.M., van Lohuizen, M., and Betticher, D.C. (2001) *Br. J. Cancer* **84**, 1372-1376
35. Voncken, J.W., Schweizer, D., Agaard, L., Sattler, L., Jantsch, M.F., and von Lohuizen, M. (1999) *J. Cell Sci.* **112**, 4627-4639
36. Min, J., Zhang, Y., and Xu, R.M. (2003) *Genes Dev*. **17**, 1823-1828
37. Yang, Y., and Herrup, K. (2005) *J. Neurosci*. **25**, 2522-2529
38. Maragakis, N.J., and Rothstein, J.D. (2006) *Nat. Clin. Pract. Neurol.* **2**, 679-689
39. Vargas, M.R., Johnson, D.A., Sirkis, D.W., Messing, A., and Johnson, J.A. (2008) *J. Neurosci*. **28**, 13574-13581
40. Nagai, M., Re, D.B., Nagata, T., Chalazonitis, A., Jessell, T.M., Wichterle, H., and Przedborski, S. (2007) *Nat. Neurosci.* **10**, 615-622
41. Otani, N., Nawashiro, H., Fukui, S., Oigawa, H., Ohsumi, A., Toyooka, T., Shima, K., Gomi, H., and Brenner, M. (2006) *J. Clin. Neurosci.* **13**, 934-938
42. Pardo, A.C., Wong, V., Benson, L.M., Dykes, M., Tanaka, K., Rothstein, J.D., and Maragakis, N.J. (2006) *Exp. Neurol.* **201**, 120-130
43. Gamaley, I.A. and Klyubin, I.V. (1999) *Int. Rev. Cytol.* **188**, 203-255
44. Kamsler, A., Daily, D., Hochman, A., Stern, N., Shiloh, Y., Rotman, G., and Barzilai, A. (2001) *Cancer Res.* **61**, 1849-1854
45. Rhee, S.G. (2006) *Science* **312**, 1882-1883
46. Yu, B.P. (1994) *Physiol. Rev.* **74**, 139-162
47. Biswas, S., Chida, A.S., and Rahman, I. (2006) *Biochem. Pharmacol.* **71**, 551-564
48. Benhar, M., Engelberg, D., and Levitzki, A. (2002) *EMBO Rep.* **3**, 420-425
49. Hyslop, P.A., Zhang, Z., Pearson, D.V., and Phebus, L.A. (1995) *Brain Res.* **671**, 181-186
50. Gottfried, C., Tramontina, F., Goncalves, D., Gonçalves, C.A., Moriguchi, E., Dias, R.D., Wofchuk, S.T., and Souza, D.O. (2002) *Mech. Ageing Dev.* **123**, 1333-1340
51. Serrano, M., Lee, H., Chin, L., Cordon-Cardo, C., Beach, D., and DePinho, R.A. (1996) *Cell* **85**, 27-37

52. Quelle, D.E., Cheng, M., Ashmun, R.A., and Sherr, C.J. (1997) *Proc. Natl. Acad. Sci. U S A.* **94**, 669-673
53. Ivanchuk, S.M., Mondal, S., Dirks, P.B., and Rutka, J.T. (2001) *J. Neurooncol.* **51**, 219-229
54. Bruggeman, S.W., Valk-Linbeek, M.E., van der Stoop, P.P., Jacobs, J.J., Kieboom, K., Tanger, E., Hulsman, D., Leung, C., Arsenijevic, Y., Marino, S., and van Lohuizen, M. (2005) *Genes Dev.* ***19***, 1438-1443
55. Burgoyne, J.R., Madhani, M., Cuello, F., Charles, R.L., Brennan, J.P., Schröder, E., Browning, D.D., Eaton, P. (2007) *Science* **317**, 1393-1397
56. Lloyd, A.C. (2006) *J. Biol.* **5**, 13

## FOOTNOTES

We thank to Lifang Zhang for providing excellent technical support for the astrocyte cultures and *Atm* mouse preparation, and Mingshan Yan, M. D. Anderson Cancer Center, for kindly providing advice and the antioxidant NAC. We also thank to Virginia Scofield for careful reading the manuscript. This project was supported by fellowship to JS Kim from the Odyssey Program of M. D. Anderson Cancer Center, and by funds from the Longevity Foundation (Formally, A-T foundation) in Austin, Texas and ATCP (A-T Children's Project).

The abbreviations used are: ATM, ataxia-telangiectasia mutated; DCFDA, 2'-7'-dichlorofluorescene diacetate; ERK1/2, extracellular signal regulated kinase1/2; MAPK, mitogen-activated protein kinase; NAC, *N*-acetyl-L-cysteine; SA *β–gal*, senescence associated *β–galactosidase*; ROS, Reactive oxygen species.

## FIGURE LEGENDS

Fig. 1. Loss of ATM impairs proliferation in astrocytes
(A) Astrocytes were isolated from the brains of newborn $Atm^{+/+}$ and $Atm^{-/-}$ mice and their growth curves were determined by trypan blue staining at indicated days after initial seeding of cells. The mean±S.D. of three independent experiments is shown. $*$, $p < 0.05$ when $Atm^{-/-}$ astrocytes were compared with $Atm^{+/+}$ astrocytes. (B) Phase-contrast photomicrographs of $Atm^{+/+}$ and $Atm^{-/-}$ astrocytes following further incubation for 4 days (left panel). ATM in C1 astrocytes was inactivated by ATM inhibitor KU55933, and knockdowned using ATM-siRNA (right panel). Scale bars = 50 μm. (C) The proportions of senescent cells in $Atm^{+/+}$ and $Atm^{-/-}$ astrocytes were determined by SA *β-galactosidase* expression 2 days after cultivation. The mean±S.D. of three independent experiments is shown. $*$, $p < 0.05$ when $Atm^{-/-}$ astrocytes were compared with $Atm^{+/+}$ astrocytes.

Fig. 2. Decreased proliferation in $Atm^{-/-}$ astrocytes is caused by elevated ROS levels
(A) $Atm^{+/+}$ and $Atm^{-/-}$ astrocytes were either left untreated or pretreated with NAC (1 mM) for 2 hours. Fluorescent $H_2$DCFDA levels were determined for these cells. The mean±S.D. of three independent experiments is shown. $*$, $p < 0.05$ when untreated $Atm^{-/-}$ culture were compared with untreated $Atm^{+/+}$ astrocytes, or when NAC-treated $Atm^{-/-}$ astrocytes were compared with untreated $Atm^{-/-}$ astrocytes. (B) Growth curves of $Atm^{-/-}$ astrocytes in the presence or absence of NAC (1 mM) were analyzed for 5 days, and then compared with those of $Atm^{+/+}$ astrocytes. The mean±S.D. of three independent counting is shown. $*$, $p < 0.05$ when NAC-treated $Atm^{-/-}$ astrocytes were compared with untreated $Atm^{-/-}$ astrocytes. (C) Photomicrographs of $Atm^{+/+}$ and $Atm^{-/-}$ astrocytes in the presence or absence of NAC. Scale bars = 50 μm. (D) Senescence of $Atm^{+/+}$ and $Atm^{-/-}$ astrocytes in the presence or absence of NAC was compared by SA *β-galactosidase* expression 2 days after cultivation. The mean±S.D. of three independent experiments is shown. $*$, $p < 0.05$ when untreated $Atm^{-/-}$ culture was compared with untreated $Atm^{+/+}$ astrocytes, or when NAC-treated $Atm^{-/-}$ astrocytes was compared with untreated $Atm^{-/-}$ astrocytes.

Fig. 3. $H_2O_2$-treated *Atm*$^{+/+}$ astrocytes show reduced proliferation and upregulated levels of CDK inhibitors

(A) *Atm*$^{+/+}$ astrocytes were pretreated with 1 mM NAC before treatment with 100 μM $H_2O_2$. Intracellular ROS levels were then measured in cultures. The mean±S.D. of three independent experiments is shown. *, $p < 0.01$ when $H_2O_2$-treated *Atm*$^{+/+}$ astrocytes was compared with untreated *Atm*$^{+/+}$ culture, or when NAC- and $H_2O_2$-treated *Atm*$^{+/+}$ astrocytes were compared with $H_2O_2$-treated *Atm*$^{+/+}$ culture. (B) *Atm*$^{+/+}$ astrocytes were pretreated with 1 mM NAC before treating with 100 μM $H_2O_2$. Photomicrographs were taken following a subsequent 4-day incubation. Scale bars = 50 μm. (C) SA *β-galactosidase* expressions in cultures from experiment (A). The mean±S.D. of three independent experiments is shown. *, $p < 0.01$ when $H_2O_2$-treated *Atm*$^{+/+}$ culture was compared with untreated *Atm*$^{+/+}$ culture, or when NAC- and $H_2O_2$-treated *Atm*$^{+/+}$ culture was compared with $H_2O_2$-treated *Atm*$^{+/+}$ culture. (D) *Atm*$^{+/+}$ astrocytes were treated with 100 μM $H_2O_2$, and then levels of p27$^{kip1}$, p21$^{cip1}$, and p16$^{Ink4a}$ were determined. The mean±S.D. of three independent experiments is shown. *, $p < 0.05$ when $H_2O_2$-treated *Atm*$^{+/+}$ astrocytes were compared with untreated *Atm*$^{+/+}$ astrocytes. (E) The effects of NAC on p21$^{cip1}$, and p16$^{Ink4a}$ expressions were determined by direct western-blotting analysis after $H_2O_2$ treatment in the presence of NAC.

Fig. 4. In *Atm*$^{-/-}$ astrocytes, ERK1/2 is constitutively activated and CDK inhibitors are upregulated

(A) For *Atm*$^{+/+}$ and *Atm*$^{-/-}$ astrocytes, levels of phospho-ERK1/2, ERK1/2, Bmi-1, and (B) levels of p53, p21$^{cip1}$, p16$^{Ink4a}$ were assessed by direct western-blotting analysis. (C) Levels of Bmi-1, p53, p21$^{cip1}$, p16$^{Ink4a}$, and phospho-Rb were compared for *Atm*$^{+/+}$ and *Atm*$^{-/-}$ cerebella tissues by direct western-blotting analysis. The mean±S.D. of three different mice tissues is shown. *, $p < 0.05$ and **, $p < 0.01$ when *Atm*$^{-/-}$ tissues was compared with *Atm*$^{+/+}$ tissues. (D) *Atm*$^{+/+}$ and *Atm*$^{-/-}$ astrocytes were treated with 100 μM $H_2O_2$. The cells were then harvested to access levels of Bmi-1 and p16$^{Ink4a}$ at the indicated times after $H_2O_2$ treatment. (E) *Atm*$^{+/+}$ and *Atm*$^{-/-}$ astrocytes were either left untreated or treated with 100 μM $H_2O_2$. Levels of phospho-ERK1/2, ERK1/2, p16$^{Ink4a}$, and phospho-Rb were determined by direct western-blotting analysis.

Fig. 5. ERK1/2 signaling mediates Bmi-1 downregulation and chromatin dissociation in *Atm*$^{-/-}$ astrocytes

(A) *Atm*$^{+/+}$ astrocytes were synchronized by contact inhibition after subculture, at which time cells were treated with 100 μM $H_2O_2$. Bmi-1 association with chromatin was analyzed by fluorescence microscope for the presence of puncta in the nucleus. p16$^{Ink4a}$ upregulation and Bmi-1/chromatin dissociation was tested using anti- p16$^{Ink4a}$ antibody. (B) Colocalization of Bmi-1 and 53BP1 was tested in the cells after $H_2O_2$ treatment using the same methods. (C) *Atm*$^{+/+}$ astrocytes were left untreated or pretreated with 50 μM PD98059 for overnight, before treating with 100 μM $H_2O_2$. The effects of 50 μM PD98059 on Bmi-1 localization in astrocytes were analyzed. (D) Photomicrographs of *Atm*$^{+/+}$ astrocytes culture from experiment (C). Scale bars = 50 μm. (E) *Atm*$^{-/-}$ astrocytes were treated with 1 mM NAC or 50 μM PD98059 for 2days. Bmi-1 expression and localization in *Atm*$^{+/+}$ and *Atm*$^{-/-}$ astrocytes were determined.

Fig. 6. Restoration of normal proliferation of Atm$^{-/-}$ astrocytes by inactivation of ERK1/2 signaling or knockdown of p16$^{Ink4a}$

(A) Growth curves of *Atm*$^{+/+}$ and *Atm*$^{-/-}$ astrocytes, cultured either in the presence or absence of 50 μM PD98059. PD98059 partially rescued *Atm*$^{-/-}$ astrocytes from defective proliferation. The mean±S.D. of three independent countings is shown. *, $p < 0.05$ when PD98059-treated *Atm*$^{-/-}$ astrocytes were compared with untreated *Atm*$^{-/-}$ astrocytes. (B) Photomicrographs of *Atm*$^{+/+}$ and *Atm*$^{-/-}$ astrocytes culture in the presence or absence of PD98059. Scale bars = 50 μm. (C) *Atm*$^{+/+}$ astrocytes were left untreated. *Atm*$^{-/-}$ astrocytes were either untreated left or treated with 1 mM NAC or 50 μM PD98059 for 2days. Levels of phospho-ERK1/2, ERK1/2, Bmi-1, p16$^{Ink4a}$, and phospho-Rb were determined by direct western-blotting analysis. (D) *Atm*$^{+/+}$ and *Atm*$^{-/-}$ astrocytes were transfected with Ink4a siRNA. p16$^{Ink4a}$ levels were determined by direct western-blotting analysis (left panel). Proportions of senescent cells were

determined by SA *β-galactosidase* expression 2 days after cultivation (right panel). The mean±S.D. of three independent experiments is shown. *, $p < 0.05$ when when untransfected $Atm^{-/-}$ astrocytes were compared with untransfected $Atm^{+/+}$ culture, or when Ink4a siRNA-transfected $Atm^{-/-}$ astrocytes were compared with untransfected $Atm^{-/-}$ astrocytes.

Fig. 7. Proposed model of a role for ATM in the maintenance of normal astrocyte proliferation

ATM is necessary to control intracellular levels of ROS. In the absence of ATM, elevated levels of ROS elicit oxidative stress and limited growth of astrocytes, through multiple ERK1/2-dependent mechanisms, including downregulation and chromatin dissociation of Bmi-1, as well as upregulation of $p16^{Ink4a}$. Abnormal proliferation of $Atm^{-/-}$ astrocytes may lead to oxidative stress in entire central nervous system, and eventually to neurodegeneration. Oxidative stress mediated-growth defects of $Atm^{-/-}$ astrocytes may be prevented by antioxidants, and normal astrocyte proliferation partially restored by inhibition of ERK1/2 signaling. Arrows denote increase or decrease when ATM is absent.

Kim,Jeesun_Fig.1

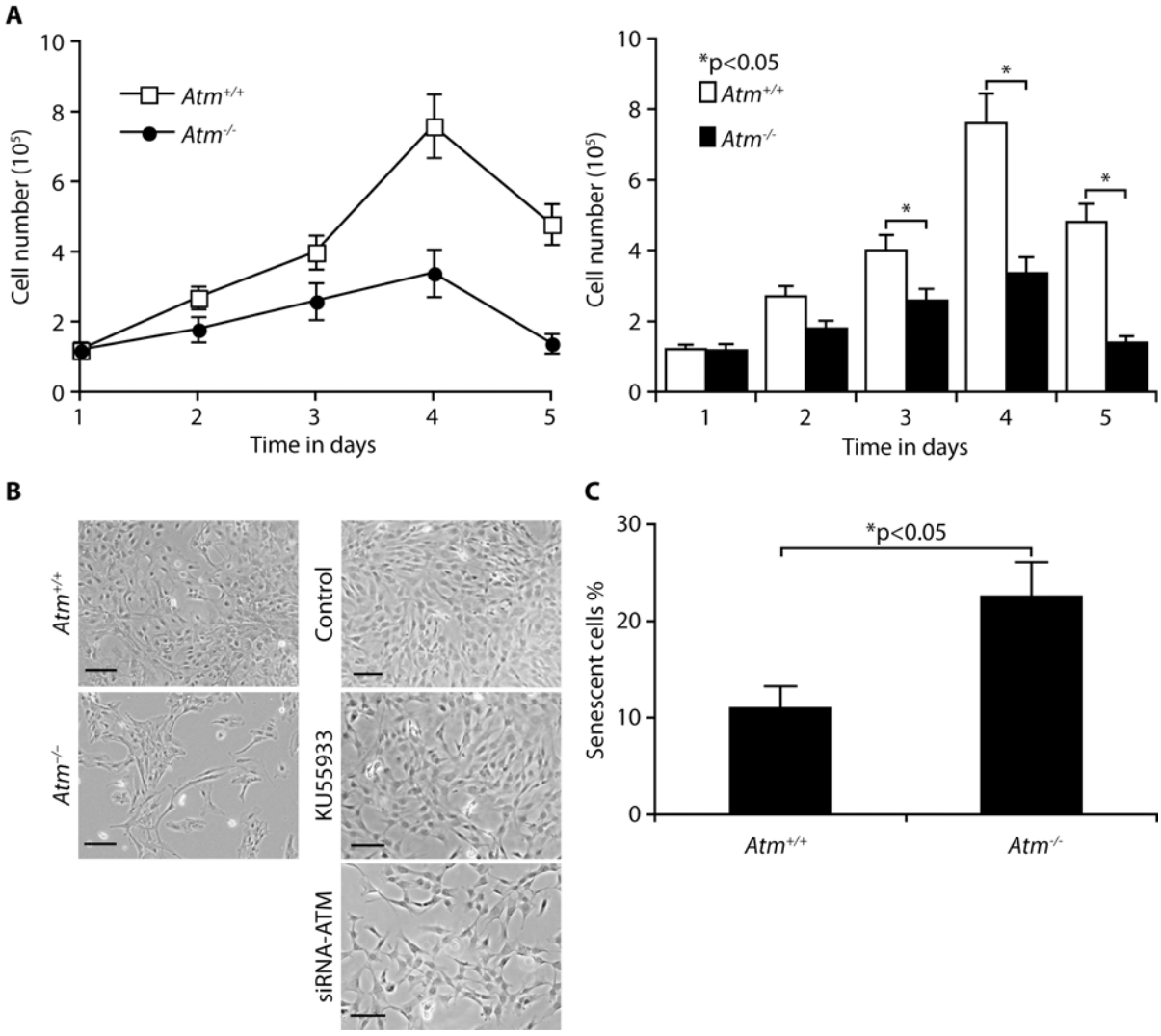

Kim, Jeesun_Fig.2

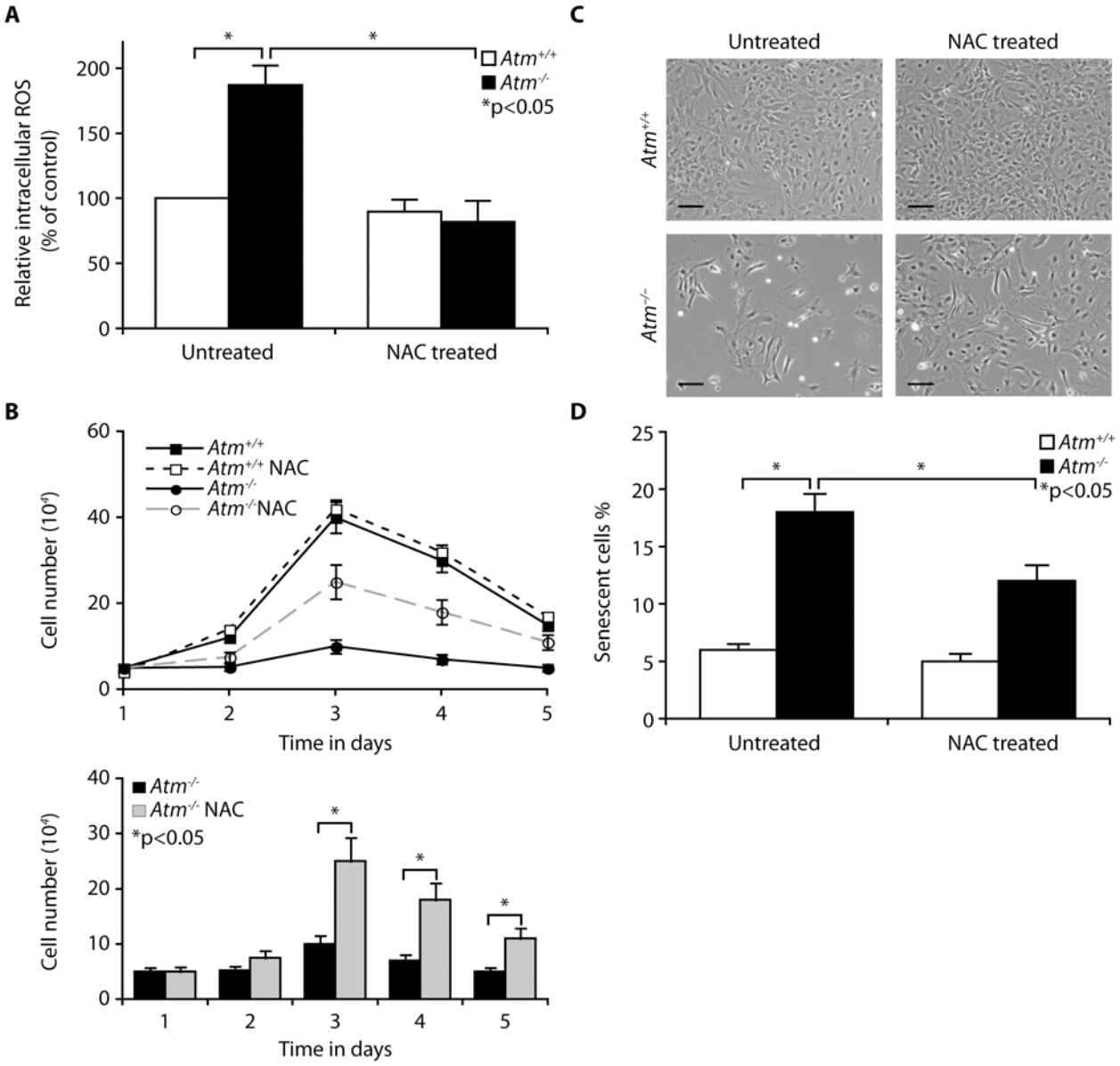

Kim, Jeesun_Fig.3

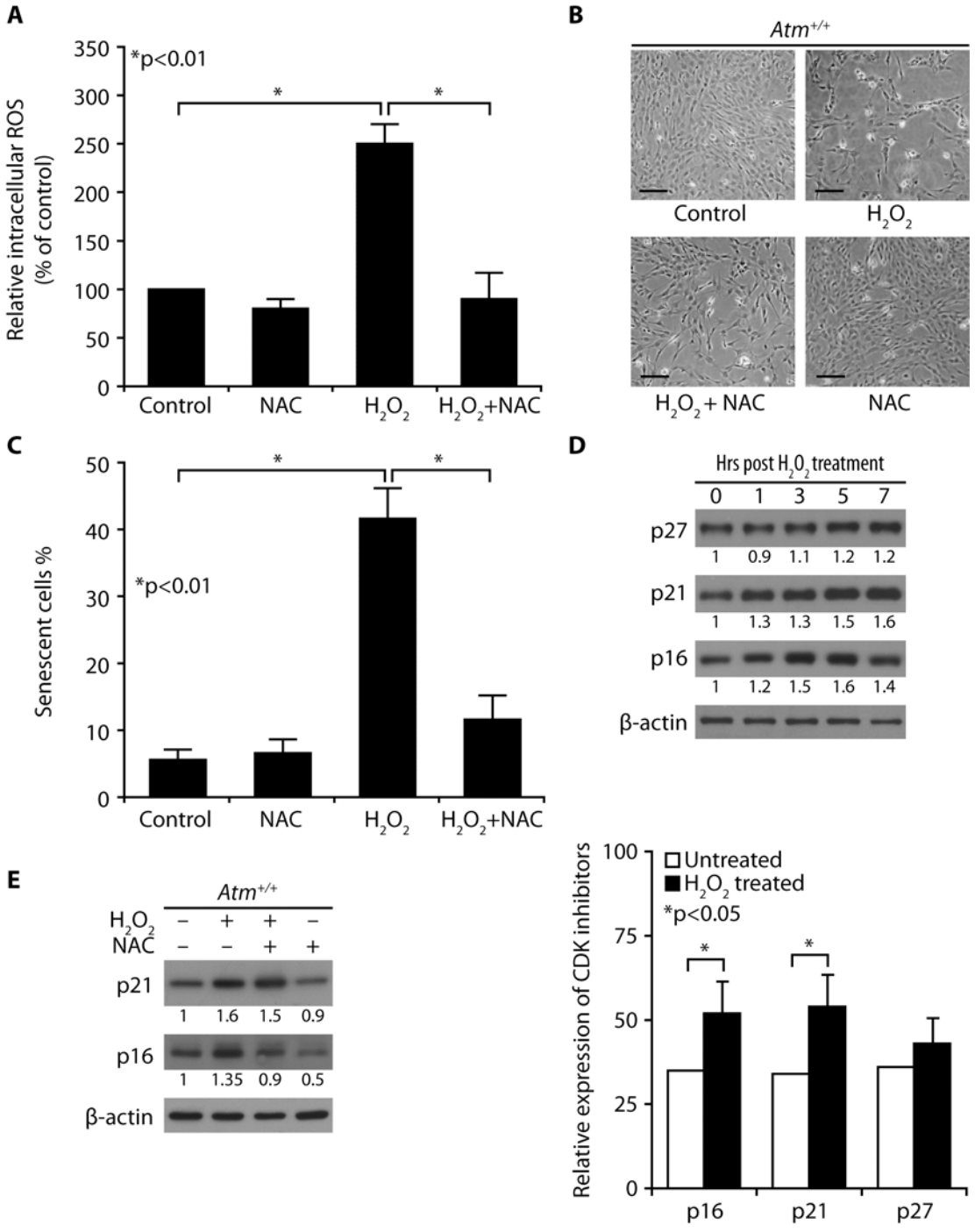

Kim, Jeesun_Fig.4

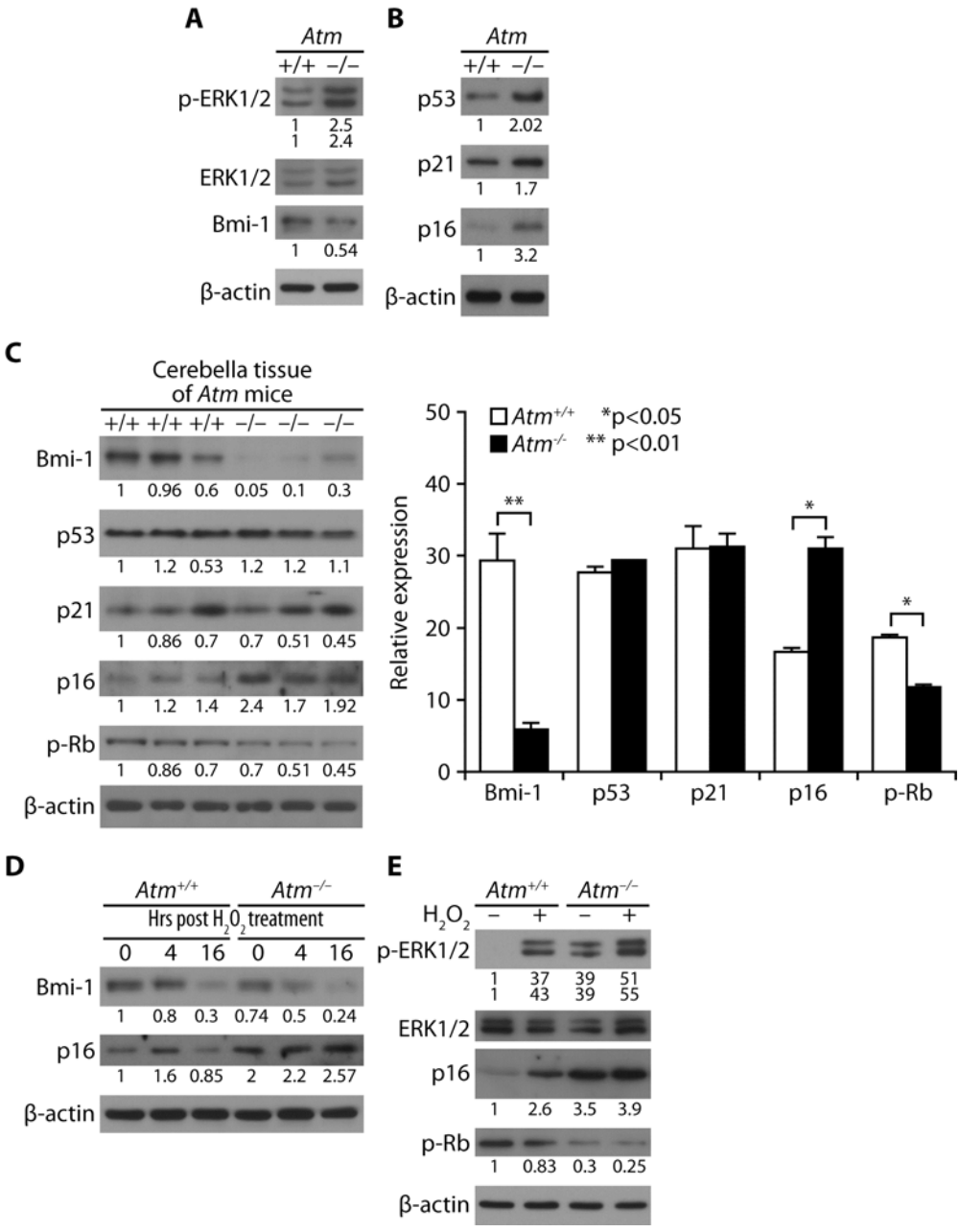

Kim, Jeesun_Fig.5

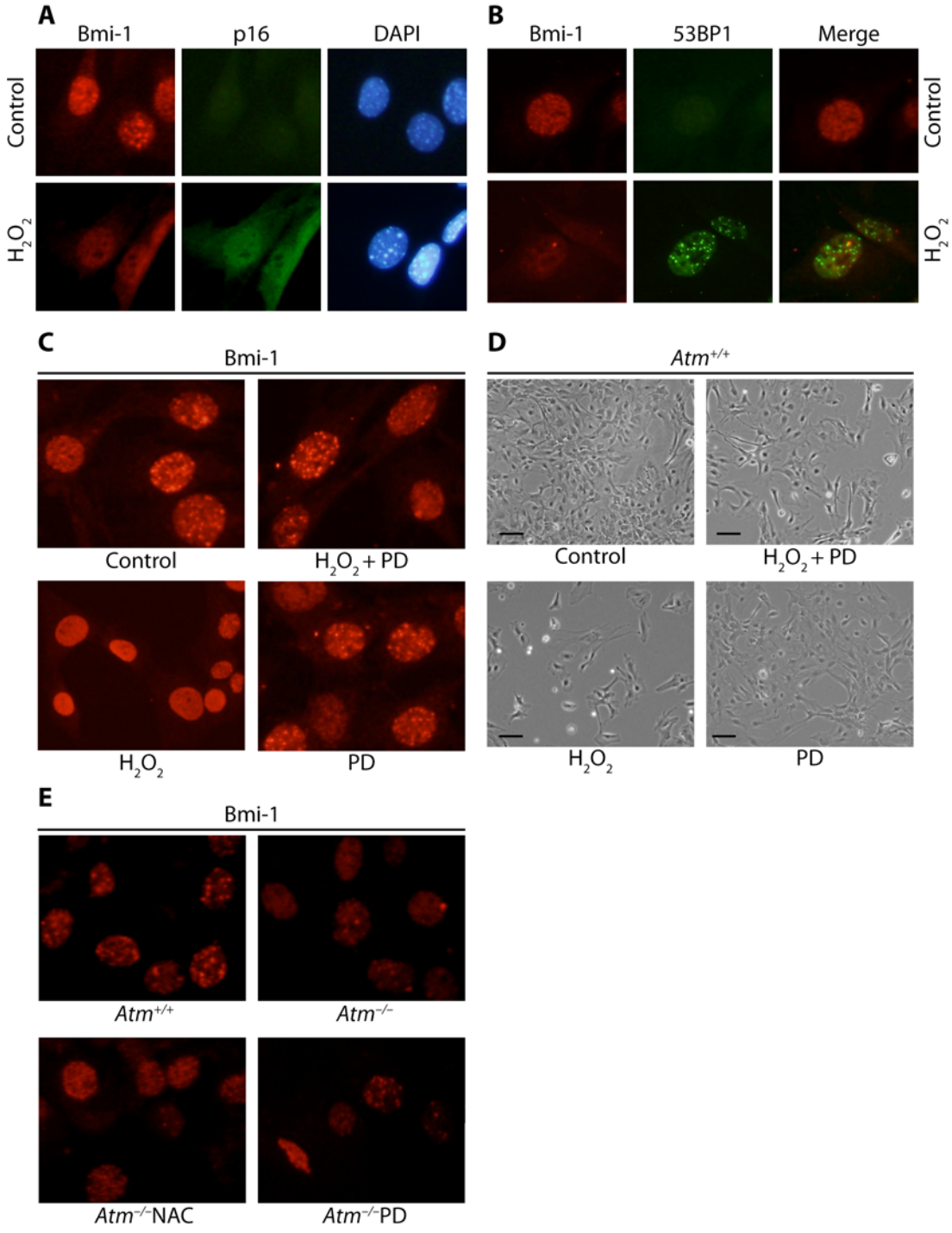

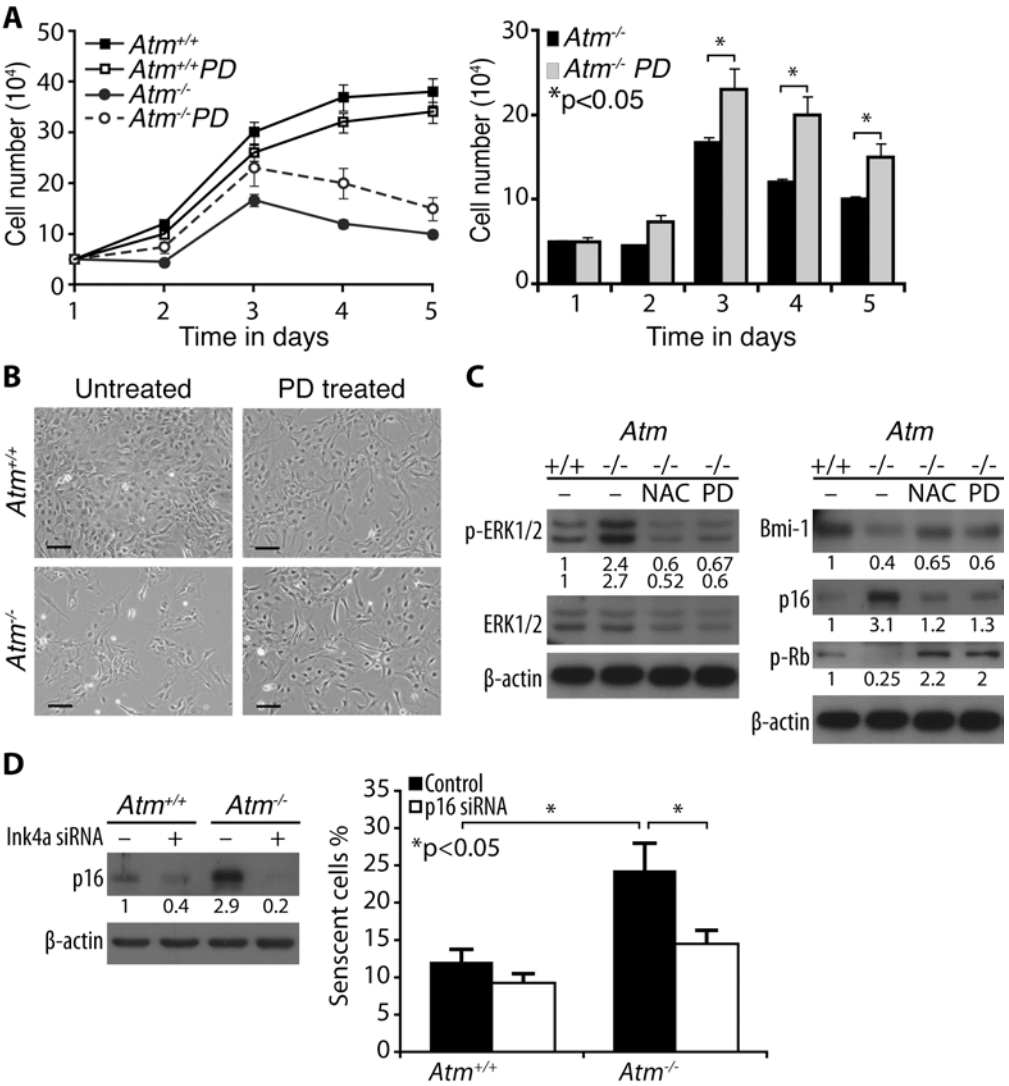

Kim, Jeesun_Fig.7